ELSEVIER

Journal of Contaminant Hydrology 38 (1999) 323–347

JOURNAL OF
Contaminant
Hydrology

Field tests and model analyses of seepage into drift

J.S.Y. Wang *, R.C. Trautz, P.J. Cook, S. Finsterle, A.L. James, J. Birkholzer

Earth Sciences Division, Lawrence Berkeley National Laboratory, MS 90-1116, One Cyclotron Road, Berkeley, CA 94720, USA

Accepted 17 November 1998

Abstract

This paper focuses on field test results and model analyses of the first set of five niche seepage tests conducted in the Exploratory Studies Facility at Yucca Mountain. The test results suggest that (1) a niche opening (short drift excavated for this study) acts as a capillary barrier; (2) a seepage threshold exists; and (3) the seepage is a fraction of the liquid released above the ceiling. Before seepage quantification, air injection and liquid release tests at two niche locations were conducted to characterize the fracture flow paths. Nearly two-order-of-magnitude changes in air permeability values were measured before and after niche excavation. The dyed liquid flow paths, together with a localized wet feature potentially associated with an ambient flow path, were mapped during dry excavation operations. After niche excavation, the seepage is quantified by the ratio of the water mass dripped into a niche to the mass released above the opening at selected borehole intervals. For the first set of five tests conducted at Niche 3650 site, the ratios range from 0% (no dripping for two tests) to 27.2%. Changes in flow path distributions and water accumulation near seepage threshold were observed on the niche ceiling. The seepage test results compare reasonably well with model results without parameter adjustments, using capillary barrier boundary condition in the niche and two-dimensional and three-dimensional conceptualizations to represent discrete fracture and fracture network for the flow paths. Model analyses of the niche tests indicate that the seepage is very sensitive to the niche boundary condition and is moderately sensitive to the heterogeneity of the fracture flow paths and to the strengths of matrix imbibition. Strong capillary strength and large storage capacity of the fracture flow paths limit the seepage. High permeability value also enhances diversion and reduces seepage for low liquid release rate.

Keywords: Drift seepage; Capillary barrier; Fracture flow paths; Tracer tests; Air permeability; Yucca Mountain

* Corresponding author. Fax: +1-510-486-6115; E-mail: jswang@lbl.gov

0169-7722/99/$ - see front matter
PII: S0169-7722(99)00019-4

1. Introduction

Scientific investigations at Yucca Mountain have contributed to the understanding of the geological framework of the site and the conceptual model of flow and transport in the unsaturated zone (Bodvarsson et al., 1999). The early conceptual model of the Yucca Mountain site (Montazer and Wilson, 1984) has been evolved and refined by systematic site scale calibration of the unsaturated state against available hydrological, temperature, and geochemical data (Bodvarsson et al., 1997). Before the completion of the Exploratory Studies Facility (ESF) for direct underground access, most of the available data and site characteristics were based on surface-based vertical boreholes. In the drifts, alcoves, and niches in the ESF, flow testing and moisture monitoring can now be carried out to acquire field data of different scales and to test different conceptual models. Capillary barrier analyses above mined openings (Philip, 1989a,b, 1990; Birkholzer and Tsang, 1997; Birkholzer et al., 1999) and between layers (Ross, 1990; Oldenburg and Pruess, 1993; Webb, 1997) can be evaluated. This paper focuses on the field tests and model analyses conducted in the ESF on capillary barrier effects of drifts.

The rate of water seepage into repository waste emplacement drifts is important for predicting performance of engineered and natural barriers. For water to seep into a drift, it needs to overcome the capillary force in the fractured tuff rock mass in order to drip into the mined opening. A seepage threshold may exist, below which no dripping will occur.

Philip et al. (1989a,b) have systematically evaluated with theoretical analyses the effectiveness of different shaped openings in porous medium as capillary barriers. At the apex and other locations on the ceiling, the accumulation of water reaching locally saturated conditions can trigger the drip–seepage processes. Capillary forces associated with the pores in the host medium can retain the water under unsaturated conditions. Local accumulation of water at the drift ceiling boundary reduces the capillary forces, and dripping can occur when the capillary forces no longer balance the gravity force. The geometric shape of the opening, the hydrological properties of the host medium, the ambient flow field and percolation flux conditions are factors determining the seepage rate and amount. Birkholzer and Tsang (1997) and Birkholzer et al. (1999) have shown with stochastic continuum models (Tsang et al., 1996) that the heterogeneity in the host medium is an important factor in determining the seepage rates. Heterogeneity enhances the occurrences of local ponding at the drift ceiling boundary. Relative humidity and other moisture conditions within the openings could also have large impacts on seepage rates.

Under steady-state conditions, the variability in pore sizes determines the saturation distribution within the rock medium, with small pores retaining the water and large pores (and fractures) remaining desaturated. However, under transient conditions induced by adding water or changing boundary conditions, connected fractures could be activated as liquid flow paths if the rock matrix with small pores and low permeability cannot imbibe water in time to remove excessive water (Wang and Narasimhan, 1985). If the flow input is episodic instead of uniform in time, allowing the pulses with large amount of water in short duration separated by long time intervals, fracture flows could occur (Nitao et al., 1992; Wang et al., 1993).

There is as yet no continuous seeping features observed along the main drift of the ESF in the Topopah Spring welded tuff unit, the host rock of the potential repository at Yucca Mountain. The seepage, or dripping, if it occurs in the future after long-term sealing of the repository without ventilation, may occur in an episodic dripping mode instead of in a continuous seepage mode. For newly excavated drifts and alcoves in ESF, drippings of construction water were observed, especially below the rock bolt holes that were drilled with water. The observed drips were associated with pressure fluctuations in mine air, and mechanical vibrations in the rock masses induced by drill and blast and other construction operations. To quantify the impact of episodic percolations on the seepage rate into drifts, liquid release tests were conducted in this drift seepage study using pulses of water.

2. Test sites

The ESF at Yucca Mountain was excavated from east to west with a tunnel boring machine from the North Portal and ramped down for over 2 km before turning to the southern direction in the potential repository level (Fig. 1). The north–south trending main drift is nearly 3.5 km long before turning east to the South Portal. The total length of ESF is 8 km and the tunnel diameter is 8 m. In the summer of 1997, two niches (short drifts of 4 m in width, 3.25 m in height, and 9 m in depth) were excavated in the northwestern direction into the west wall along the main drift of the ESF to test seepage processes and to observe flow paths. Niche 3566 (3566 m from the ESF North Portal) is located between the Sundance Fault and a reactivated cooling joint. Bomb pulse samples with elevated $^{36}Cl/Cl$ ratios were found on rock fragments collected at both the fault and the joint (Fabryka-Martin et al., 1996). Niche 3650 (3650 m from the ESF North Portal) is located in a relatively competent rock mass, with an apparent lower fracture density and simpler fracture pattern than the site at Niche 3566.

3. Air permeability distributions

The air injection (pneumatic) tests were conducted before and after niche excavation. Before niche excavations, three 10-m long horizontal boreholes were drilled at Niche 3566, and seven boreholes were drilled at Niche 3650. The boreholes were drilled from the ESF main drift in the northwestern direction into the wall at three levels, with the upper-level boreholes above the future niche space (Fig. 2).

At each site, cross-hole pneumatic tests were conducted in boreholes instrumented with packers to map out the permeability field (Chapter 2 by Cook et al. in Wang et al., 1997). The packer assemblies have multiple rubber-gland sections on 5 cm (2 in.) diameter tubes. The injection packer assemblies are 3.4 m (11 ft) long, with five internal zones (0.3 m or 1 ft long) and one end zone. Each zone has two ports on opposite sides

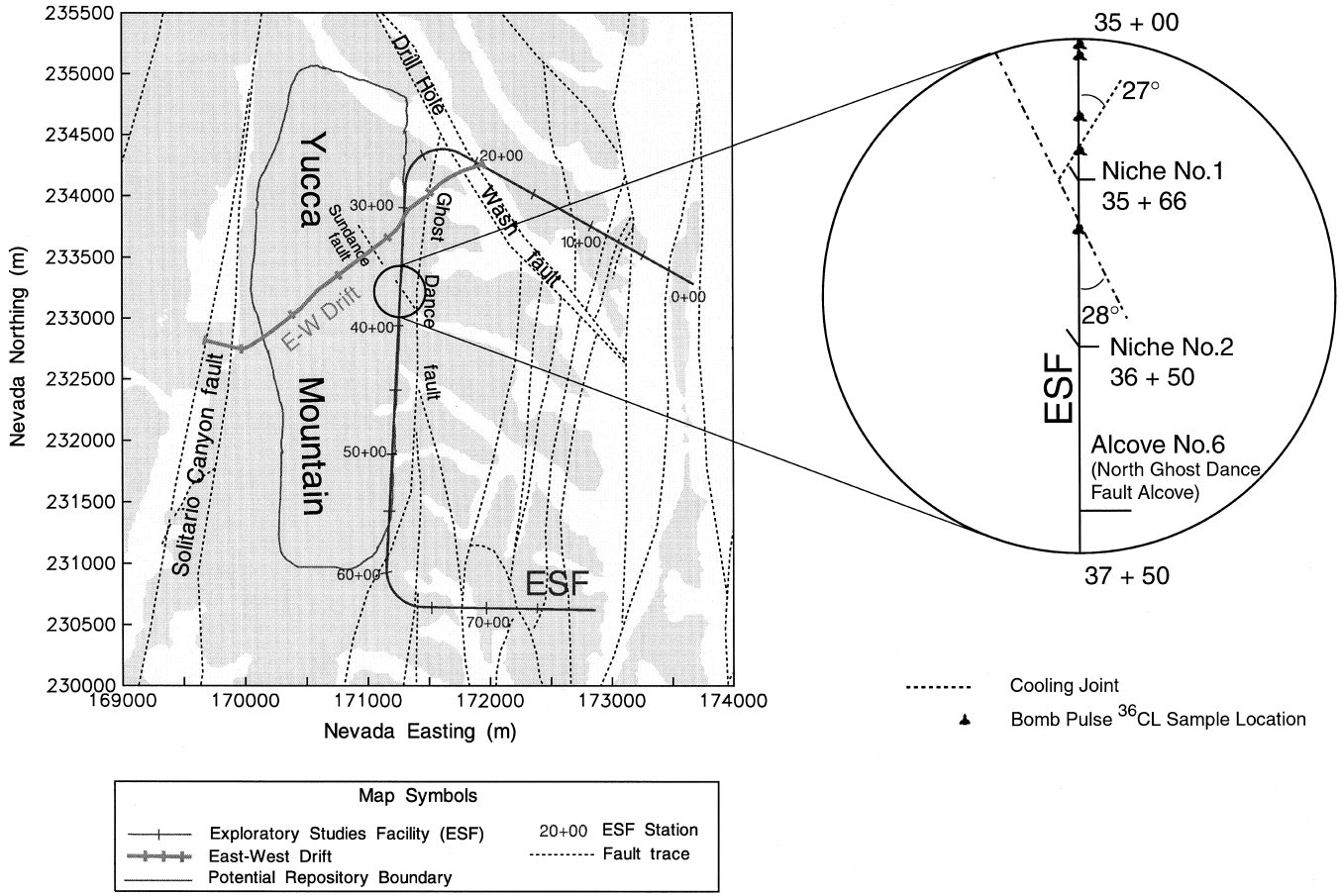

Fig. 1. Location map of Niche 3566 near the Sundance Fault and Niche 3650 between Sundance Fault and Alcove 6.

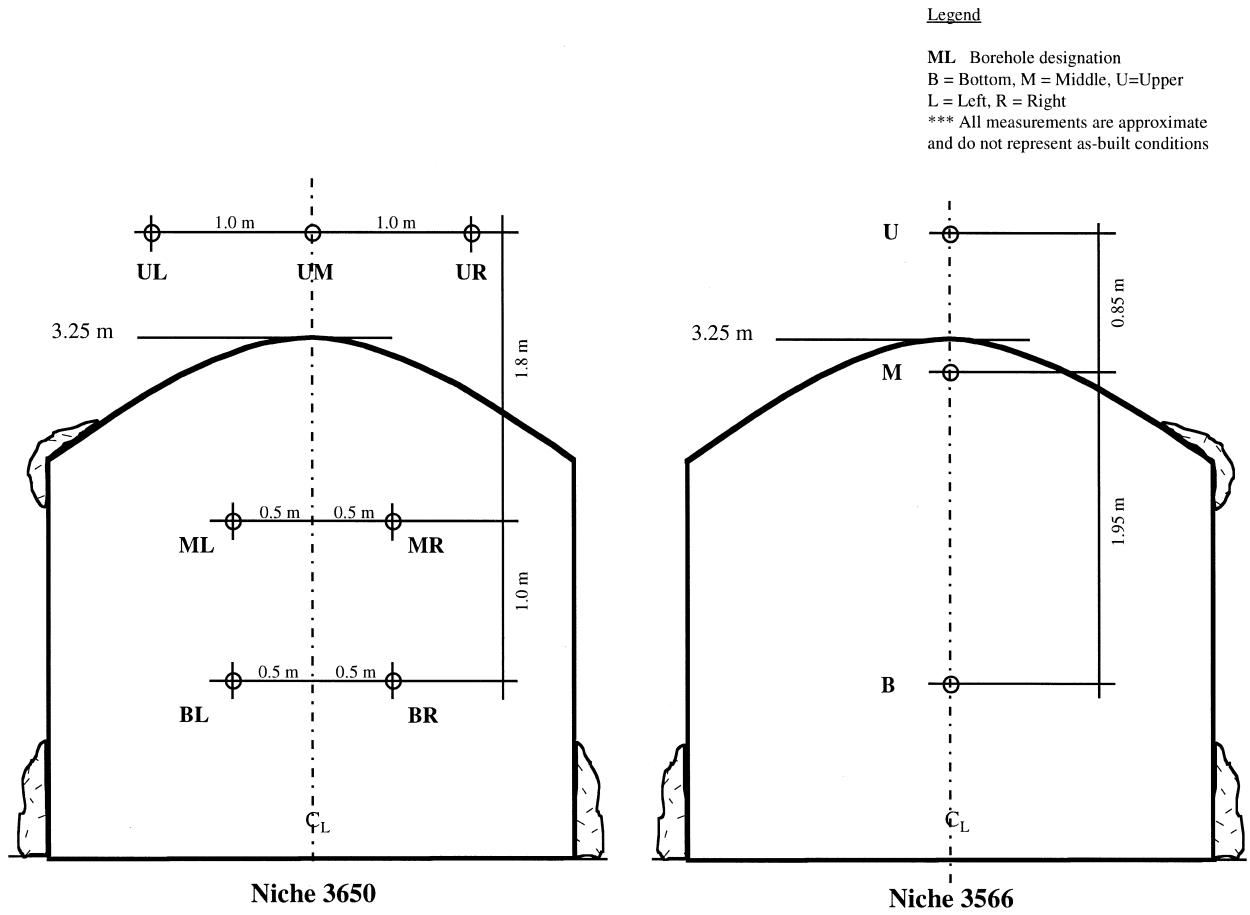

Fig. 2. End view of boreholes on the wall of ESF main drift before Niche 3566 and Niche 3650 were excavated.

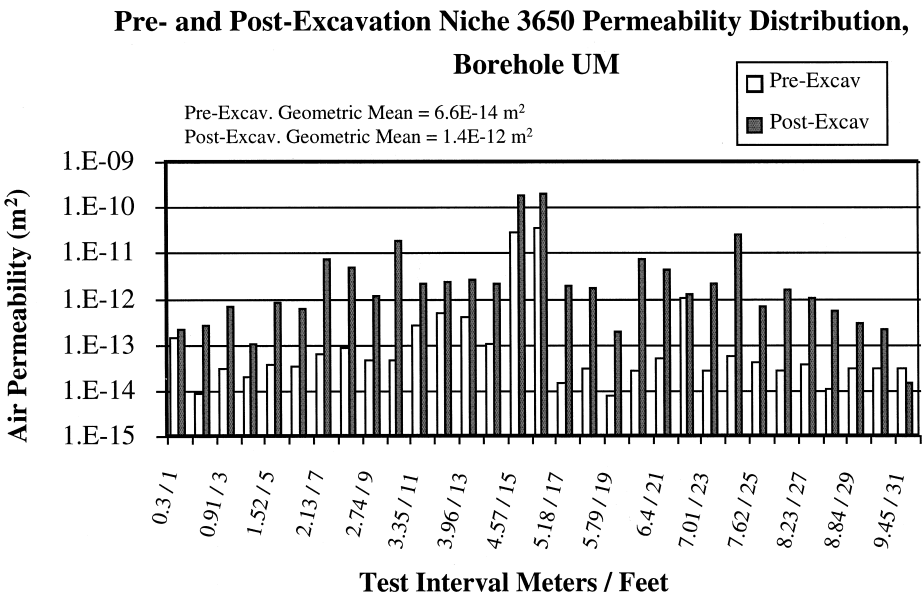

Fig. 3. Permeability distribution along the upper middle borehole at Niche 3650 before and after niche excavation.

of the packer tube body, one for injection and one for pressure sensing. The observation packer assemblies are 6.1 m (20 ft) long, with 10 internal zones and one end zone with one port each zone for pressure sensing. Permutations of different packer locations were used to map out the permeability field with spatial resolution of 0.3 m (1 ft).

Fig. 3 illustrates an example of the permeability distribution measured along the upper middle (UM) borehole at Niche 3650. The pre-excavation permeability values of this borehole range from 7.2×10^{-15} m^2 to 3.2×10^{-11} m^2, with the geometric mean of 6.6×10^{-14} m^2. The borehole interval permeability distributions, together with the cross-hole pressure changes observed in the air injection tests, were used to select the intervals for liquid-release tests.

After niche construction, the permeability values for most of the borehole intervals increased. The post-excavation permeability values in borehole UM range from 1.3×10^{-14} m^2 to 1.9×10^{-10} m^2, with the geometric mean of 1.4×10^{-12} m^2. This is likely due to fractures being opened up by the stress relief associated with niche excavation, resulting in a mechanically induced enhancement in permeability values. A secondary cause for the changes in permeability values could be the proximity of the

Fig. 4. Distribution of flow paths in Niche 3566: (a) blue-dyed flow paths along fractures; (b) red-dyed flow paths through multiple fractures; (c) damp feature in a brecciated zone in the vicinity of the Sundance Fault.

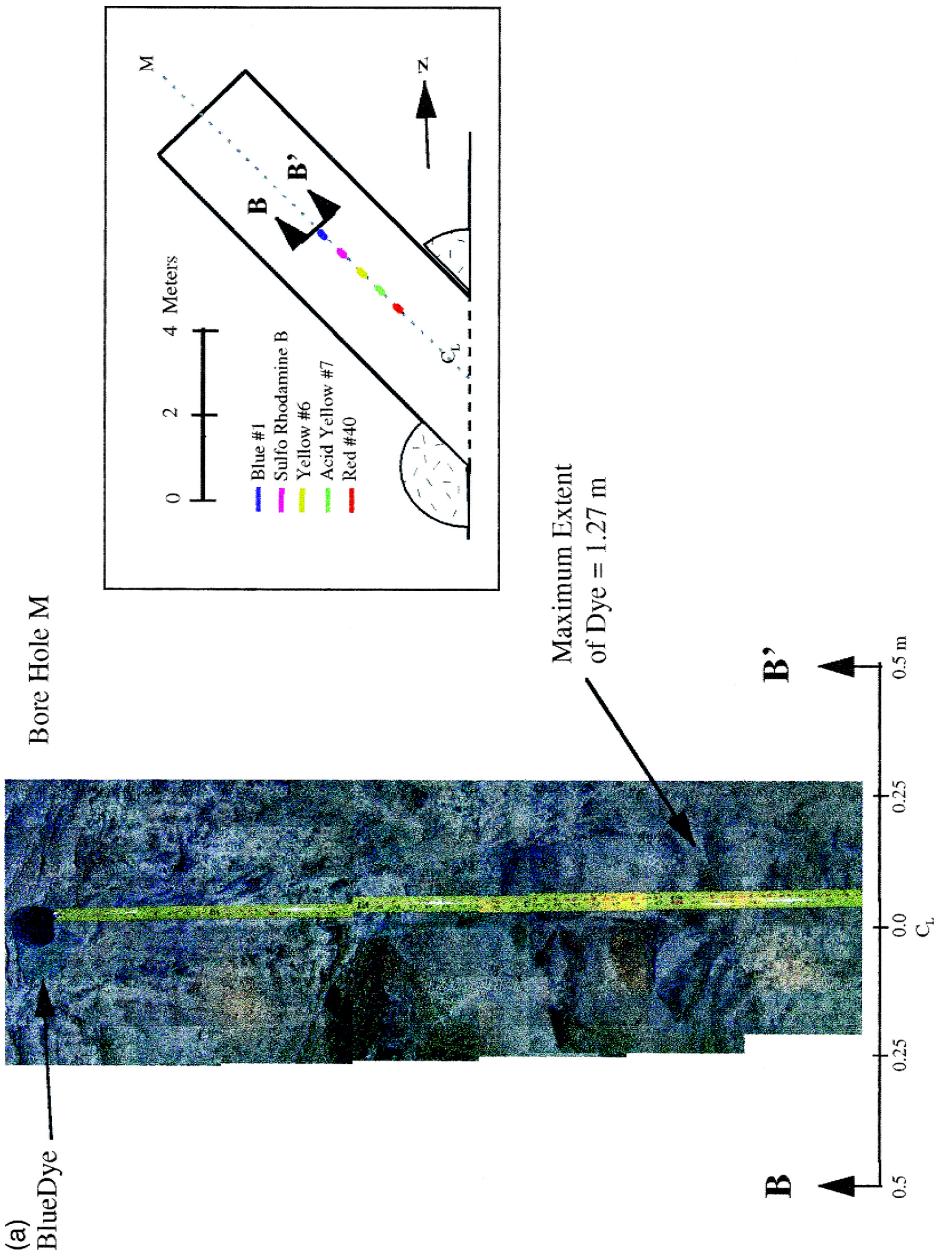
(a)
BlueDye
Bore Hole M
Maximum Extent
of Dye = 1.27 m
B
B'
0.5
0.25
0.0
0.25
0.5 m
C_L
M
B
B'
N
0
2
4 Meters
Blue #1
Sulfo Rhodamine B
Yellow #6
Acid Yellow #7
Red #40
C_L

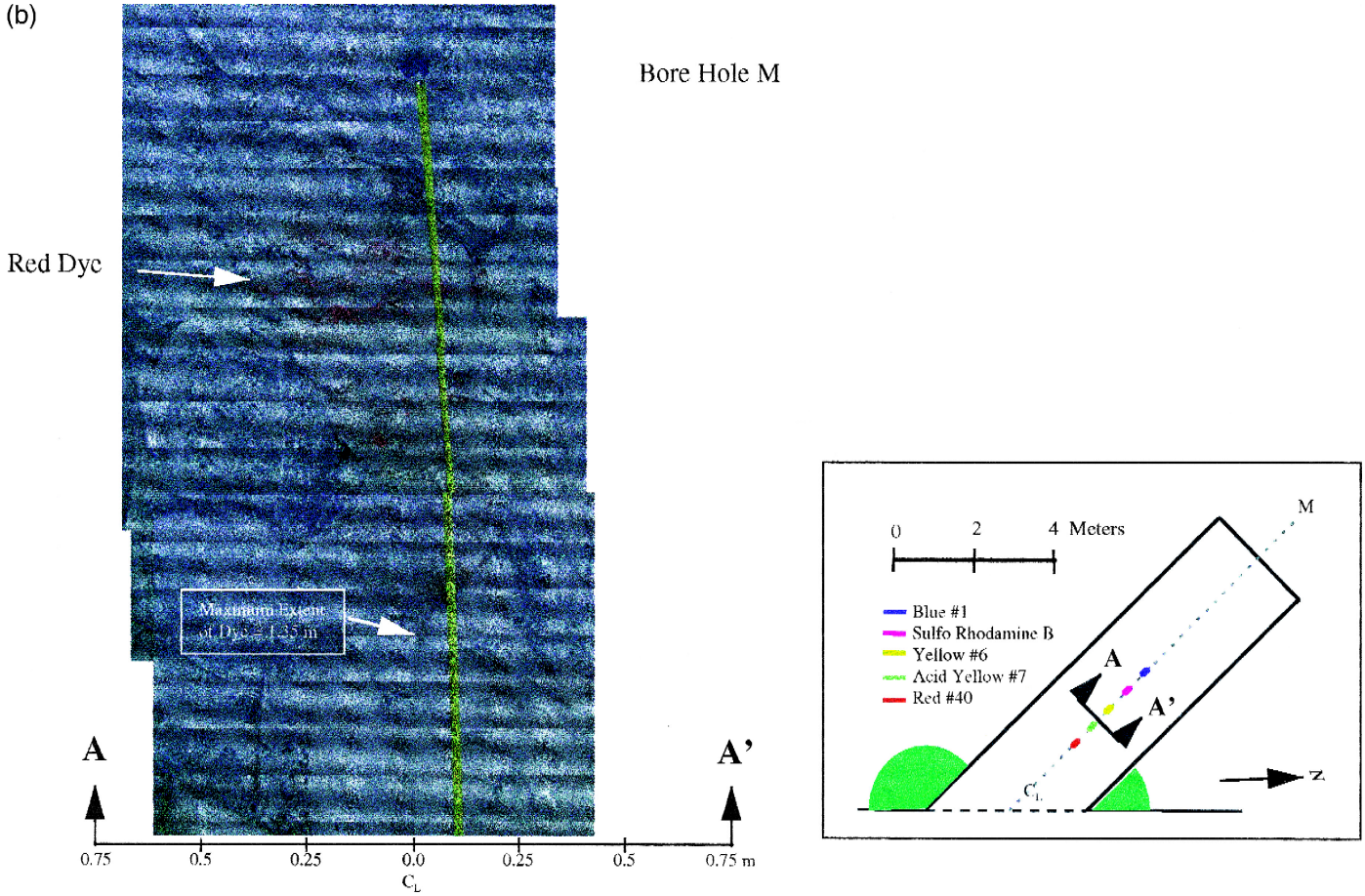

Fig. 4 (continued).

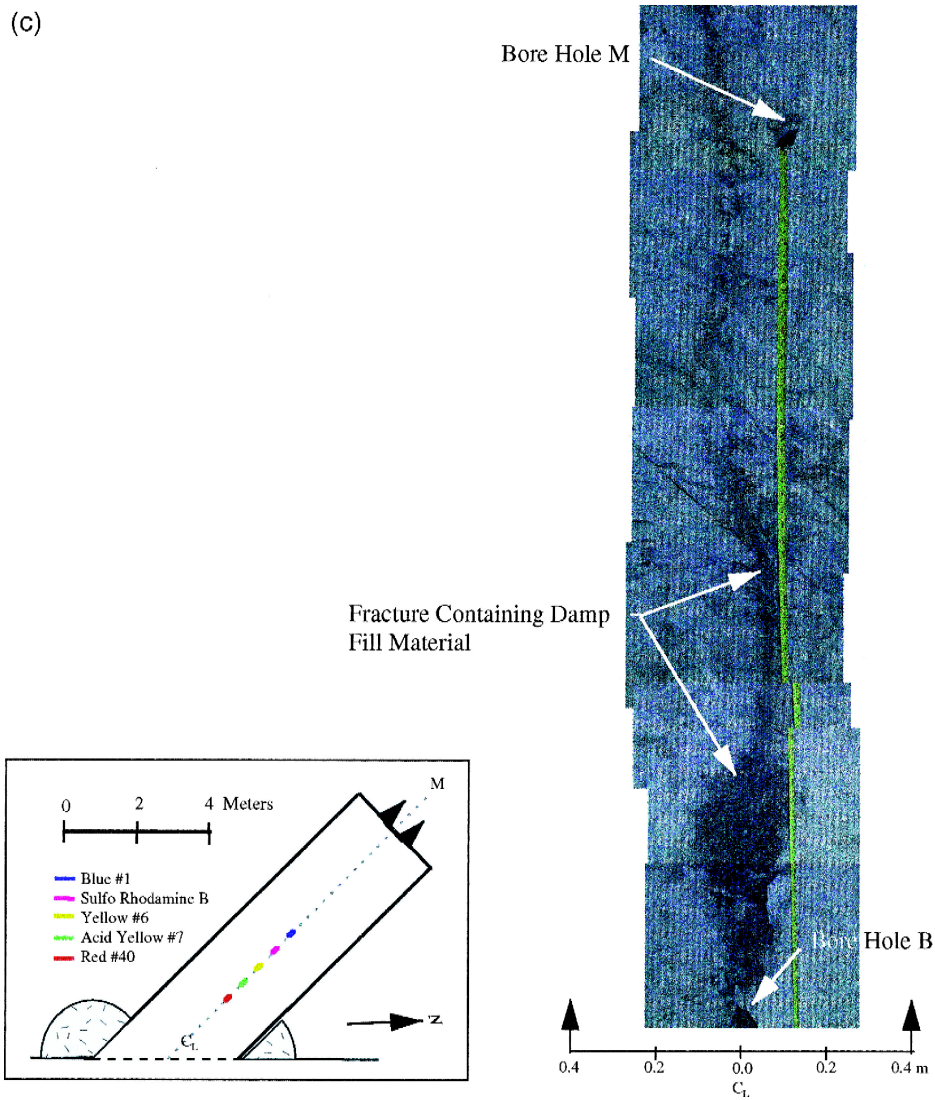

Fig. 4 (continued).

niche open boundary which may affect the analysis based on a steady state line source solution (LeCain, 1995).

4. Liquid flow paths

Pre-excavation liquid release tests were conducted in the middle borehole at Niche 3566 and in three upper boreholes and two middle boreholes at Niche 3650. The liquid release tests were carried out with finite volumes of dye-spiked water injected at

selected borehole intervals using the same pneumatic injection packer assemblies. The distributions of dye-traced flow paths were mapped during niche excavations. During dry-niche excavation operations within 2 to 3 weeks after liquid releases, photographs of the dyed flow paths were taken, and grab samples were collected (Chapter 3 by Trautz et al. in Wang et al., 1997). Different flow path patterns were observed, with dye stains observed either on a few nearly vertical discrete fractures (as illustrated in Fig. 4a), or associated with a network of fractures dispersing the plume (as illustrated in Fig. 4b).

These montaged photographic images are from the tests conducted at Niche 3566, with tracers released in the middle (M) borehole (Fig. 2). Fig. 4a and b are examples of tests using dyes approved for use in food, drugs, and cosmetics (FD&C) by the U.S. Food and Drug Administration. Color additives Blue No. 1 and Red No. 40 were dissolved in water and released into borehole test intervals. The niches were constructed dry with multiple cuts of 0.3–0.7 m advances and photographs were taken between the cuts. With the rock surrounding and below borehole M removed through multiple cuts, it is generally possible to have several sets of images of the dyed flow paths on newly excavated faces. The blue-dyed paths originated from the release of 474 g of water were observed in two mined depths (Fig. 4a is one example), with maximum penetration depth (vertical distance from injection interval to the observed dye location) of 1.3 m and maximum lateral extent of 0.46 m. The red-dyed paths originated from the release of 941.7 g of water were observed in three mined depths (Fig. 4b is one example), with maximum penetration depth of 1.52 m and maximum lateral extent of 0.54 m.

A nearly vertical wet feature without dye stains was also observed at the end of Niche 3566, extending from the niche ceiling to the floor, as illustrated in Fig. 4c (Wang et al., 1997). This feature could represent an ambient flow path, with the length over 3 m and the average width less than 0.3 m (1 ft). The damp feature is in a brecciated zone in the vicinity of the Sundance Fault. The feature essentially dried up in hours. The observation of this damp flow path substantiates the test condition adapted in the drift seepage tests, with localized releases of water into borehole intervals of 0.3 m (1 ft) length.

5. Seepage tests

This paper focuses on the five tests conducted along the UM borehole at Niche 3650. After niche excavation at Niche 3650, the liquid-release tests were repeated in the borehole intervals tested before niche excavation. The test intervals selected for both the pre-excavation and post-excavation liquid release tests, together with averaged injection rates and injected volumes, are given in Table 1.

Within a packer interval, the air injection port on the packer tube pointing in the downward direction was used as a liquid-injection port. The air-pressure sensor port on the packer tube pointing upward was used as a liquid return port. If the liquid injection rate was higher than the capacity of the test interval to take the water, excessive water can flow freely out the test interval. The maximum water level buildup within a test interval is 5 cm (2 in.), which is the elevation difference between the ports on the packer tube. Of the five pre-niche liquid release tests conducted along the UM borehole at

Table 1
Liquid release test intervals, air permeability values, and mass injection rates and volumes along the upper middle borehole at Niche 3650

Test number	1	2	3	4	5
Injection zone	4.27–4.57 m (14–15 ft)	4.88–5.18 m (16–17 ft)	5.49–5.79 m (18–19 ft)	6.10–6.40 m (20–21 ft)	6.70–7.01 m (22–23 ft)
Pre-excavation					
Air permeability (m^2)	9.2×10^{-14}	3.2×10^{-11}	2.8×10^{-14}	2.5×10^{-14}	9.2×10^{-13}
Average rate of injection (g/s)[a]	−0.0146	−2.85	−0.24	−0.049	−0.89
Injected mass (g)	675.8	937.4	115.7	106.8	438.7
Post-excavation					
Air permeability (m^2)	2.0×10^{-12}	1.9×10^{-10}	1.6×10^{-12}	7.0×10^{-12}	1.1×10^{-12}
Average rate of injection (g/s)[a,b]	−2.02	−2.89	−2.07	−0.51	−0.56
Injected mass (g)[b]	1008.7	1033.1	1013.4	1000.3	274.5

[a] Derived from net injection mass divided by injection time.
[b] With line storage corrections ($< 3\%$) taken into account.

Niche 3650, return flows were observed in three out of five test intervals. In post-excavation tests, return flow was observed only in one out of five test intervals. The fracture system after excavation can take in water more easily than the ambient system before excavation.

For the pre-excavation liquid release tests at Niche 3650, an alternating sequence of blue- and red-colored dyes was employed starting with Blue No. 1 in the first test interval (Test no. 1) located 4.27–4.57 m (14–15 ft) from the collar of the borehole. For Test no. 1, the dyed flow paths were observed in four mined depths, with maximum penetration depth of 1.68 m and maximum lateral extent of 0.87 m. The corresponding values for Test no. 2 are: two observations, 0.86 m maximum penetration, 0.37 m lateral extent; and for Test no. 5: six observations, 1.82 m penetration, and 0.81 m maximum lateral extent. During excavation, the colored dyes from Test no. 3 and Test no. 4 were not observed in the niche. The observations of dyes during niche excavation indicated that the injected mass for the corresponding test intervals migrated over 0.65 m, the distance from the borehole to the niche ceiling. Front edges of plumes were observed above the niche floor. The majority of injected dyes were excavated out of the niche space.

After niche excavation, a 3.4 m (11 ft) × 4.9 m (16 ft) liquid capture system, divided into 0.3 m × 0.3 m (1 ft × 1 ft) sections, was installed below the ceiling at Niche 3650. With a fluid collection system installed below the ceiling, the total mass of flow seeping into the niche can be measured. In the tests with dripping observed, the majority of the water were collected in one or two of the 176 (11 by 16) compartments. In general, once the wetting front arrived at the niche ceiling through the fracture system, limited lateral spreading along the ceiling surface and capillary imbibition into small aperture fractures were observed. Drippings were observed shortly (14 to 122 s) after wetting front arrivals in the cases where measurable seepages occurred.

Test results of the percentage of injected water dripping into the niche are illustrated in Fig. 5. Test no. 5 (6.70–7.01 m or 22–23 ft interval) did not induce dripping into the

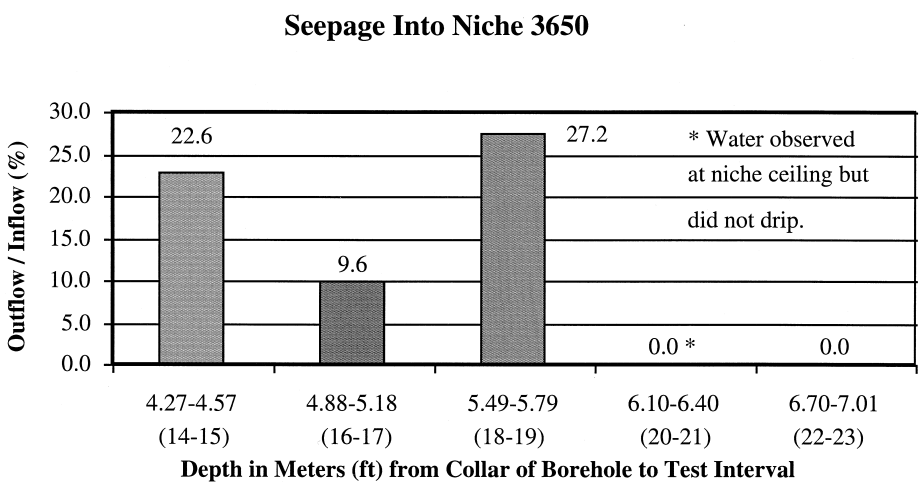

Fig. 5. Ratio (in %) of seepage observed in the niche and inflow injected above the niche along the upper middle borehole at Niche 3650.

niche. Test no. 4 (6.10–6.40 m or 20–21 ft interval) induced flow to reach the ceiling, with flow observed to stay or migrate along on the ceiling surfaces instead of dripping into the niche. Fluorescent dyes (Pyranine—green, Sulfo Rhodamine B—pinkish purple, Amino G Acid—blue, Acid Yellow no. 7—greenish yellow) were used in the post-excavation tests so that the flow paths from post-excavation tests could be clearly distinguished with ultraviolet illumination from the food dyes of the pre-excavation tests observable under ambient lights.

Fig. 6a–c are examples of photographs of the wetted area on the ceiling of the niche. The flow paths in the post-excavation tests (with fluorescent dyes) did not necessarily correspond to the wetted area (food dye stained area) created by the pre-excavation tests. In several instances, including the graphic examples from test intervals 4.27–4.57 m (14–15 ft), 4.88–5.18 m (16–17 ft), and 6.10–6.40 m (20–21 ft), water was observed draining from or moving through fractures that did not conduct water before the niche was excavated. The changes in liquid flow paths are related to the changes in fracture network due to excavation as indicated by the increases in air permeability values presented earlier in Fig. 3. The liquid injection rates and injected mass also increase from pre-excavation test conditions to the post-excavation test conditions, as illustrated in Table 1. The large increases in transient liquid injection rates, together with large increase in air permeability values, support the interpretation that fracture flow paths were altered by niche excavation.

Fig. 6. Photographs of the ceiling of Niche 3650 showing the wetting fronts from post-excavation liquid release tests (using fluorescent dyes) and stained areas from pre-excavation tests (using food dyes): (a) Test no. 1; (b) Test no. 2; and (c) Test no. 4. (Dark green and bright orange lines were surveyor's markers).

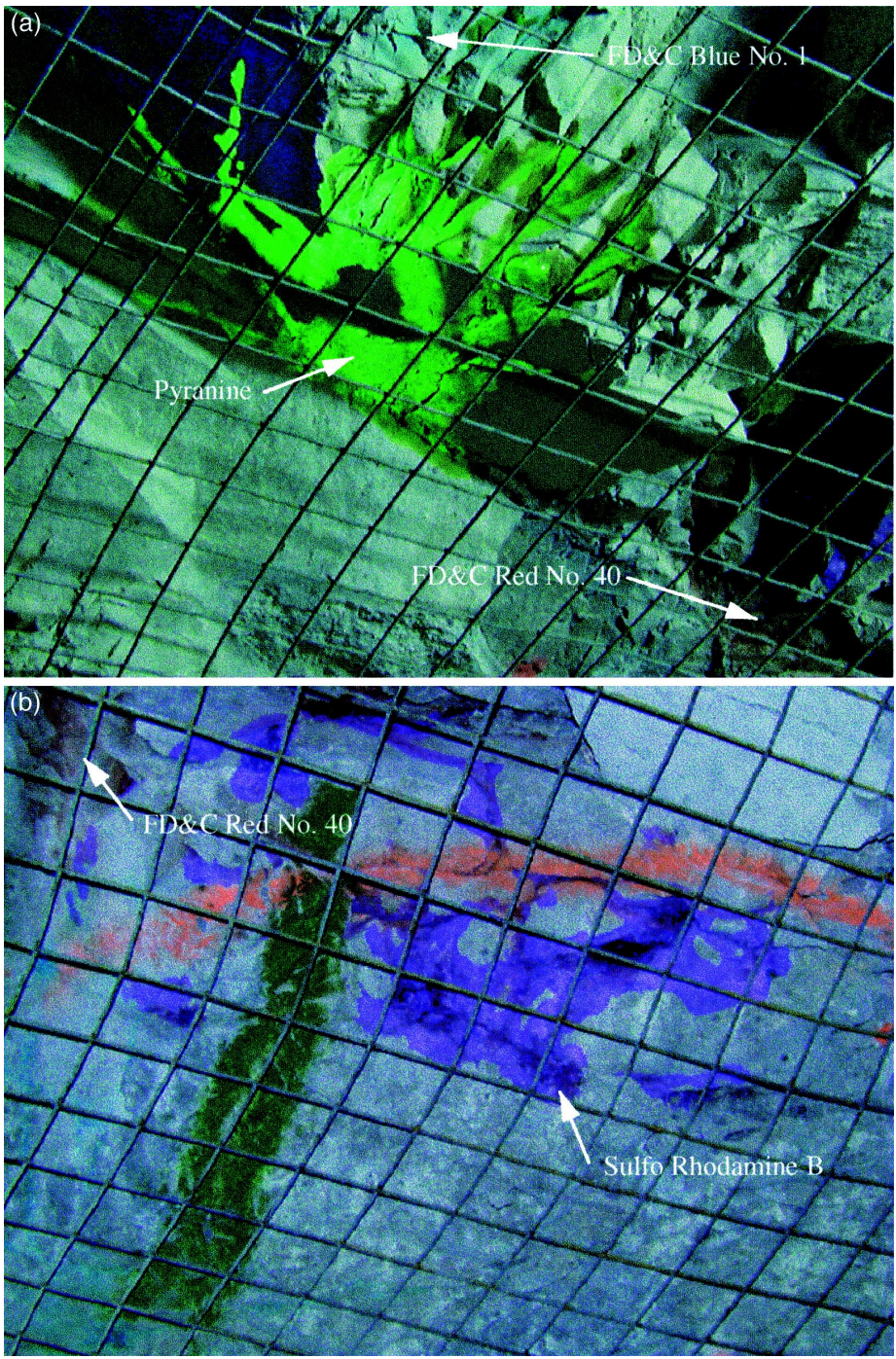
(a)
FD&C Blue No. 1
Pyranine
FD&C Red No. 40
(b)
FD&C Red No. 40
Sulfo Rhodamine B

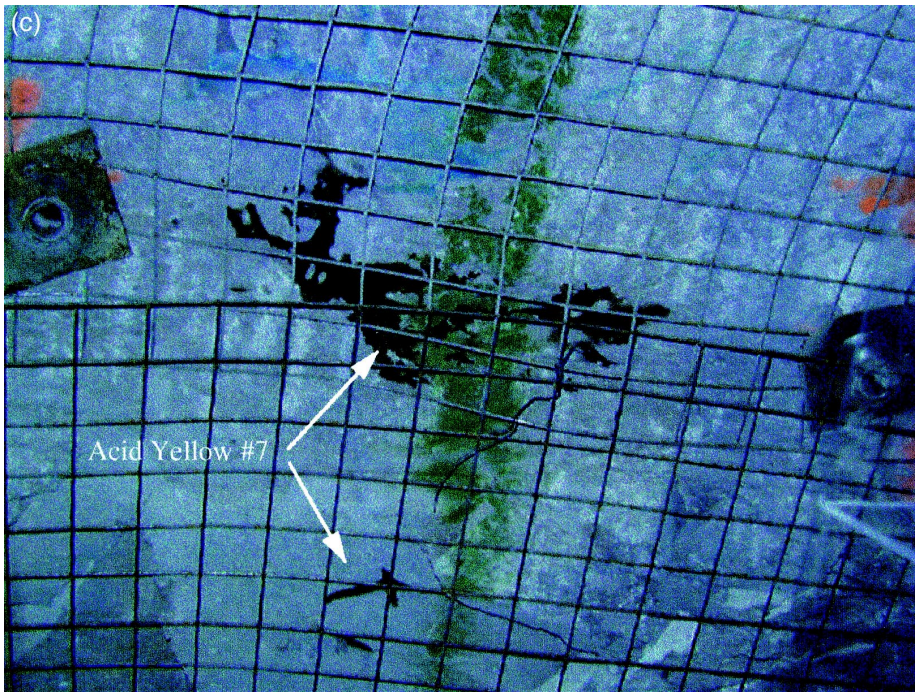

Fig. 6 (continued).

Fig. 6c is for Test no. 4, (6.1–6.4 m or 20–21 ft), with wetting front observed to arrive on the ceiling but no dripping occurred. After the initial flow breakthrough at fracture traces, water was observed to migrate along the surface, imbibe into other small fractures, and stay on the niche ceiling. Local saturated conditions were likely not achieved to initiate the dripping process. The pre-excavation dyed water (with Red No. 40) released into the borehole interval was not observed on the niche ceiling, indicating that original fracture flow paths were too tight to substantiate migration over 0.65 m, the distance from the borehole to the niche ceiling. With niche excavation opening up the fracture flow paths, released liquid (with Acid Yellow no. 7 fluorescent dye) can move to the ceiling, but not fast or massive enough to initiate dripping. The blue-dyed areas in Fig. 6c were associated with release of the neighboring test interval. The other dark green and orange lines in Fig. 6a–c were paints applied by the mine surveyors during excavation, and not related to the dyed liquid release tests.

In this set of liquid release tests, the test interval from 4.88 to 5.18 m (16 to 17 ft; Test no. 2) with the highest permeability value along the UM borehole did not induce the highest percentage of seepage into the niche. Fractures with high permeabilities may enhance diversion, reduce seepage, and require large liquid volumes or high flow rates to induce a locally saturated condition at the fracture outlet on the niche ceiling. The seepage does not always occur at the most obvious fracture in the vicinity of the

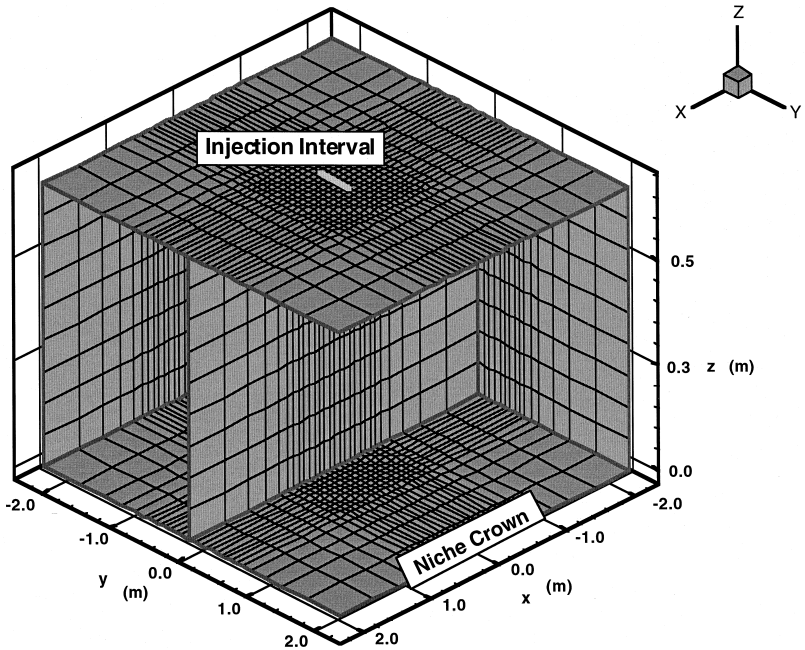

Fig. 7. Three-dimensional mesh for the region between the injection interval and the niche ceiling for liquid release tests and seepage determinations.

dripping points. In this high-permeability test interval, the liquid release rate is not sensitive to excavation induced changes. For the case with liquid release rate lower than

Table 2
Comparison of niche seepage test results with drift scale model results

Test number	1	2	3	4	5
Post-excavation permeability (m^2)	2.0×10^{-12}	1.9×10^{-10}	1.6×10^{-12}	7.0×10^{-12}	1.1×10^{-12}
Seepage percentage					
Test result	22.6%	9.6%	27.2%	0%[a]	0%
Model result	20.7%	5.4%[b]	19.6%	0%	0%
First arrival time (min)					
Test result	6.93	3.00	3.47	34.5[a]	NA
Model result	5.3	3.9[b]	6.3	NA	NA
Duration of dripping (min)					
Test result	33.83	NR	17.63	NA	NA
Model result	12.8	2.0[b]	15.0	NA	NA

[a]Liquid flow arrival was observed on the niche ceiling, no dripping.
[b]An isotropic permeability assumed.
NA: not applicable.
NR: not recorded.

Table 3
Sensitivity of seepage percentage to different conceptual models for Test no. 3

Test no. 3 result	27.2%
Base homogeneous model	19.6%
Scaled heterogeneous model	34.7%
Matrix imbibition, $1/\alpha_m = 0.156$ MPa	15.9%
Matrix imbibition, $1/\alpha_m = 1.56$ MPa	10.6%
Free drainage boundary	87.4%

the hydraulic conductivity of the flow paths, the seepage percentage decreases as permeability increases.

6. Niche model analysis

In the first series of models for the five liquid release tests, a three-dimensional fracture continuum model is used, as illustrated in Fig. 7, for the region between the injection interval and the niche ceiling. For each test interval, the fracture permeability value from the corresponding air permeability test is assigned for the whole model domain. Other parameters are fracture porosity value of 0.1%, a van Genuchten capillarity parameter $1/\alpha_f$ of 1000 Pa, and a van Genuchten pore-size distribution parameter n_f of 2.7. These drift-scale 'primary-case' parameters were developed for Total System Performance Assessment input (Tsang et al., 1997) from the unsaturated zone site scale model (Bodvarsson et al., 1997). No parameter adjustment or calibration was performed in this series of calculations to test drift scale seepage models. The niche is treated as a capillary barrier, with a relative humidity of 100% assumed at the ceiling boundary, at the immediate vicinity of the dripping points.

Table 2 compares the model results with seepage test results, including the seepage percentages in Fig. 5, the first arrival times, and the duration of dripping. Overall, the agreement with the test results is good, considering that no parameter adjustment was made. For Test nos. 1 and 3, the seepage percentage and the timing of seepage into the niche are well-represented by the model. The model results also agree with the two test cases no. 4 and no. 5 with no dripping. For Test no. 2 with high permeability value, the first model estimates predicted that there would be no seepage with this three-dimensional model. However, if the high permeability value was associated with a discrete vertical fracture connecting the borehole interval to the niche ceiling, a two-dimensional model might be better suited for the interpretation of this test. This concept is adapted in the model by assigning anisotropic permeability structure with a two-order-of-magnitude smaller permeability in one horizontal direction. With this conceptualization, the match between model results and test results is quite good.

Fig. 8. Saturation distributions after 8.22 min for Test no. 3 condition with (a) homogeneous permeability field, and (b) heterogeneous permeability field.

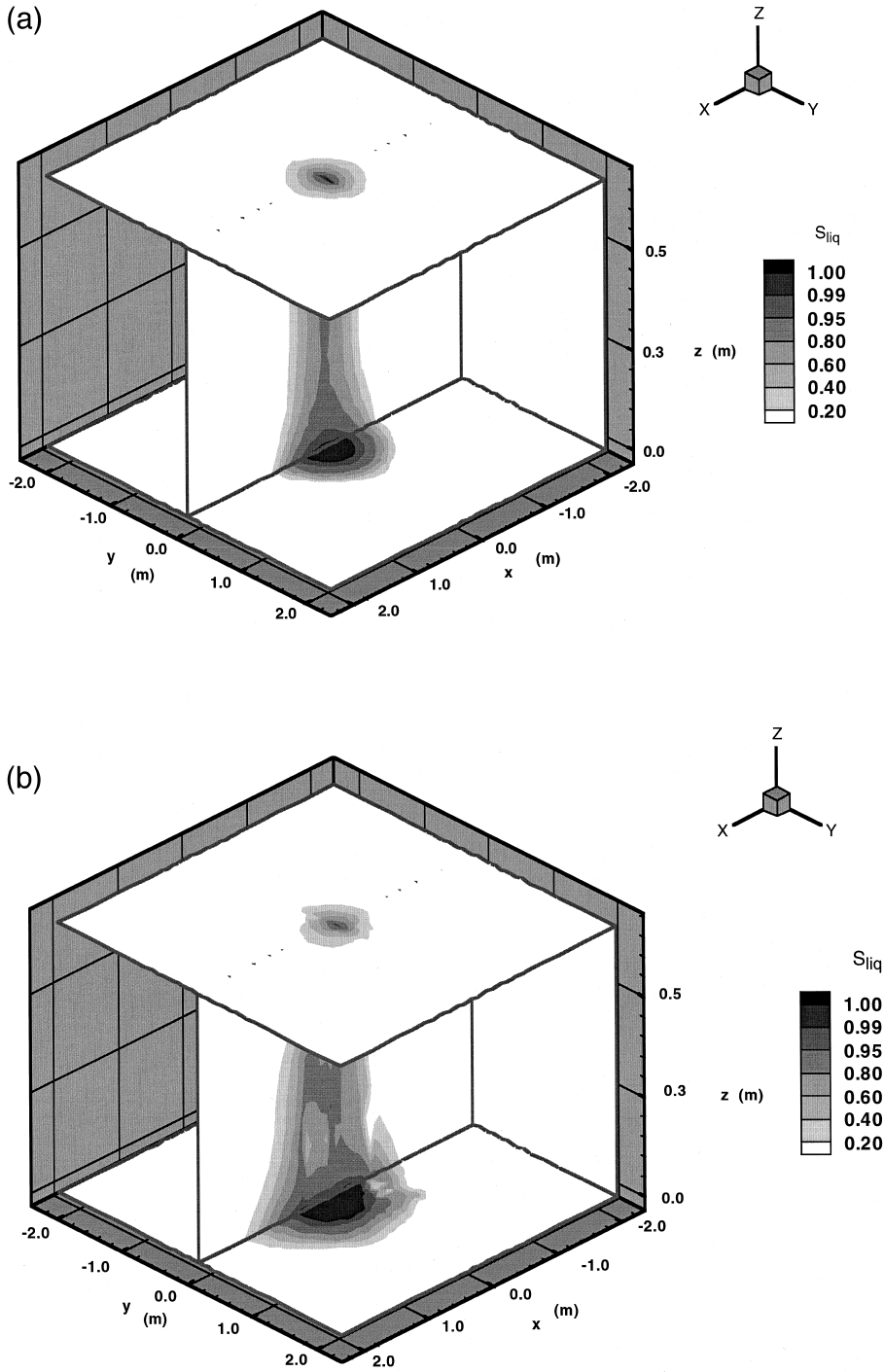
(a)
Z
X
Y
S_{liq}
1.00
0.99
0.95
0.80
0.60
0.40
0.20
z (m)
0.5
0.3
0.0
-2.0
-1.0
0.0
1.0
2.0
y (m)
x (m)
(b)
Z
X
Y
S_{liq}
1.00
0.99
0.95
0.80
0.60
0.40
0.20
z (m)
0.5
0.3
0.0
-2.0
-1.0
0.0
1.0
2.0
y (m)
x (m)

Additional sensitivity studies for different conceptual models were performed for the Test no. 3 condition, as summarized in Table 3. The homogeneous permeability model is replaced by a heterogeneous field derived from the field used in the drift scale model, with all permeability values scaled to arrive at a geometric mean equal to the measured air permeability value. The correlation length is also scaled down to 0.33 m, a reasonable value at this site based on permeability variation along the niche boreholes (Fig. 3). The heterogeneity increases the seepage percentage to 34.7%, from the homogeneous case result of 19.6%. The corresponding field test result is 27.2%. The heterogeneity induces wider spread of the plume and enhances the creation of local saturated conditions at the niche boundary, as illustrated in Fig. 8a for the homogeneous case and Fig. 8b for the heterogeneous case.

The matrix imbibition effects were evaluated using a multiple interacting continuum model (Pruess and Narasimhan, 1985), with the matrix block represented by four nested interacting continua. The full geometric interface between fracture and matrix block is assumed in the model to maximize the matrix imbibition effects. The matrix properties are representative for the tsw34 unit at Yucca Mountain (Bodvarsson et al., 1997). Two cases using different matrix capillarity parameters were considered, one with $1/\alpha_m$ of 1.56 MPa, the tsw34 value, the other using 10% of this value. The model results indicate that the matrix imbibition reduces the seepage for a few percent for the short distances and durations in the niche test conditions. Preliminary inspection of grab samples collected in the niches does not show substantial dye penetration into the rock matrix. Dyes were observed mainly in fractures and on fracture surfaces.

The seepage is sensitive to niche boundary conditions. If the niche boundary is assumed to be a free drainage boundary, with liquid arriving at the boundary readily draining into the drift without requiring local ponding conditions to initiate dripping (i.e., no capillary barrier effect), the seepage percentage is much higher than the base case with the capillary barrier boundary condition. The field observations of water accumulation on the niche ceiling before dripping (and in one case with no dripping) support the model that the niche opening acts as a capillary barrier.

7. Parameter sensitivity analysis

Parameter sensitivity analyses were carried out with both two-dimensional and three-dimensional models to represent discrete fractures and fracture network surrounding the niche. Two-dimensional models were developed for test design before niche excavation and liquid release tests to determine the sensitivity of liquid-plume migrations on the fracture parameters, injection volumes, and rates (Chapter 4 by Finsterle et al. in Wang et al., 1997). The models are extended to a larger range of sensitive parameters, using refined two- and three-dimensional models. In the parameter sensitivity analyses, a total of 1000 g of water is injected in 500 s at a rate of 2 g/s is assumed. For the base case parameter set (permeability $k_f = 10^{-12}$ m^2, fracture porosity $\phi_f = 10^{-3}$, van Genuchten capillary parameter, $1/\alpha_f = 1000$ Pa), the two-dimensional saturation distributions after 10, 30, 60, and 120 min are shown in Fig. 9.

From the base case parameter set, permeability and porosity were changed by one order of magnitude, and the van Genuchten parameter (van Genuchten, 1980) by half an

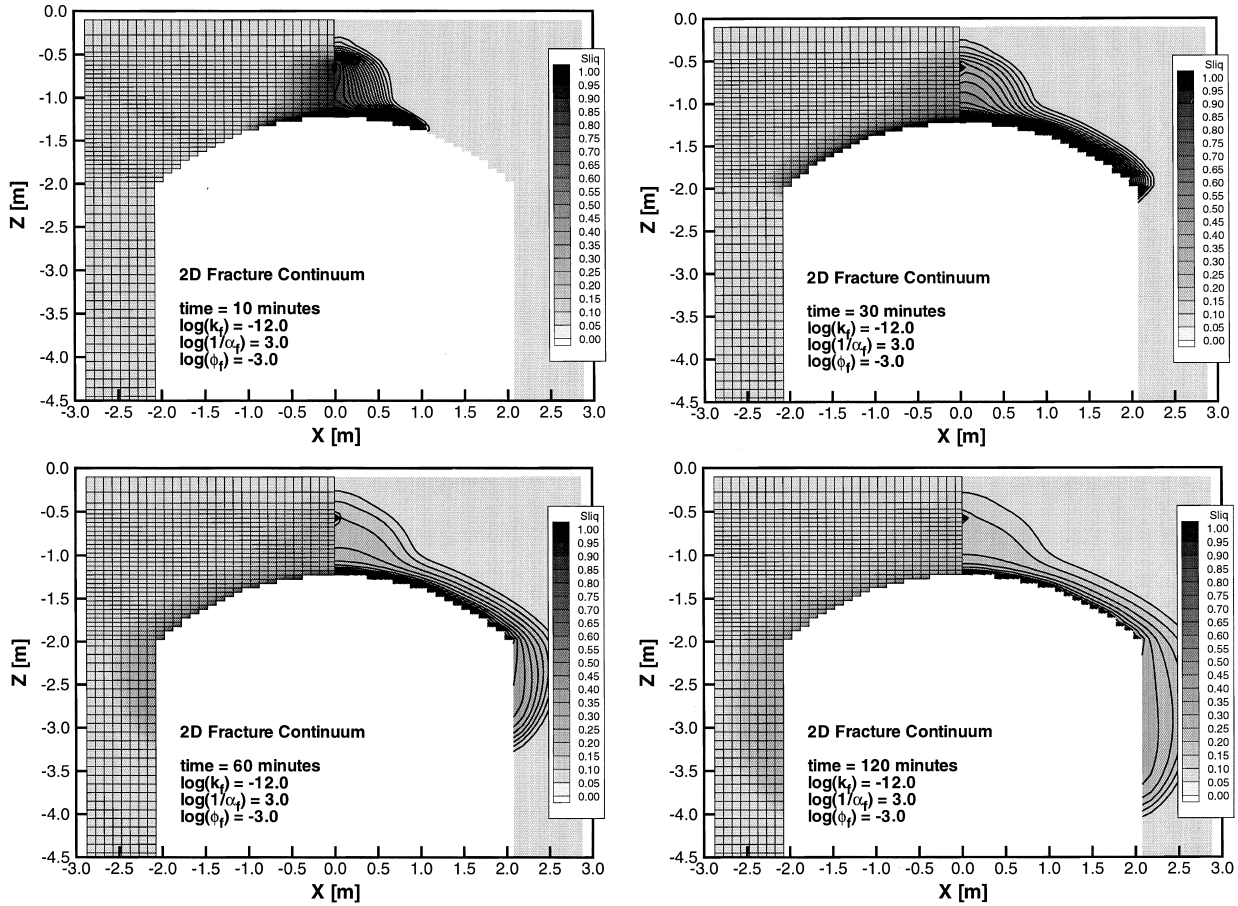

Fig. 9. Saturation distributions after 10, 30, 60, and 120 min, with base case parameters.

order of magnitude, respectively. Fig. 10 illustrates the sensitivity of transient behavior. As compared with the base case parameter set, increase in permeability, reduction in porosity, and increase in capillarity lead to faster breakthrough. However, transient behavior is not correlated with final amount of seepage. For example, high permeability enhances breakthrough but reduces the total seepage. Combinations in parameters can result in seepage percentages ranging from 0% to nearly 90%.

Reducing permeability results in slower plume migration, but higher average plume saturation. High saturations are required to overcome the capillary barrier acting at the niche boundary. Consequently, the amount of water seeping into the niche is higher for low permeabilities than for high permeabilities. For stronger capillary forces, plume spreading is increased, resulting in lower overall saturations and less seepage. The effectiveness of capillary barrier is increased with increasing formation capillarity. The higher the fracture porosity, the more water can be held in the formation by capillarity, leading to reduced seepage. Plume migration is slower for higher porosity.

Seepage is large for rock formations with low permeability, low capillarity, and low porosity. The sensitivity analysis is carried out with the ITOUGH2 code (Finsterle, 1997). Using the seepage percentage after 1 day as the measure of total seepage, the sensitivity of the seepage percentage as a function of porosity, permeability, and capillarity is summarized in Fig. 11. High porosity, representing the large storage

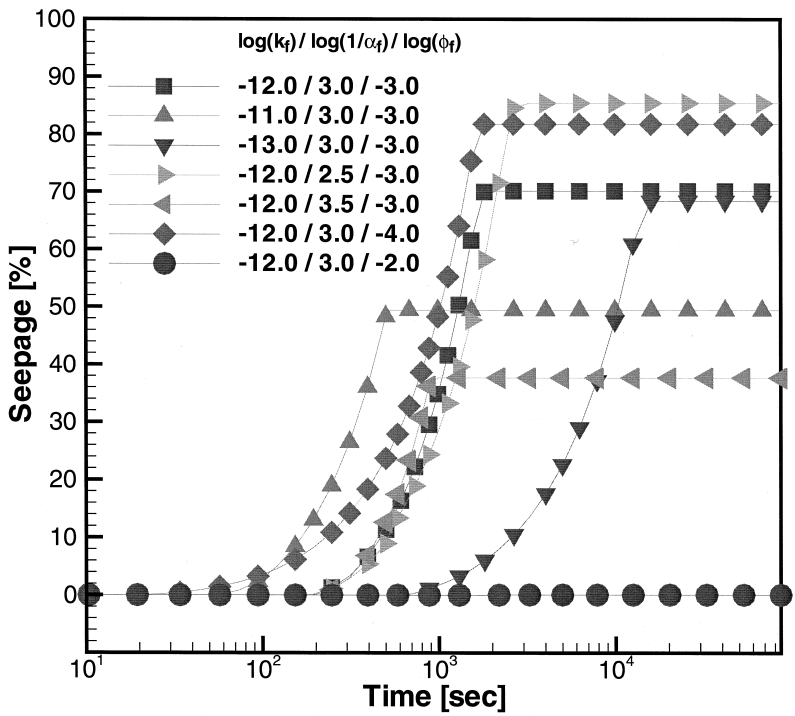

Fig. 10. Transient behavior of seven different parameter combinations. The first combination is the base case parameter set.

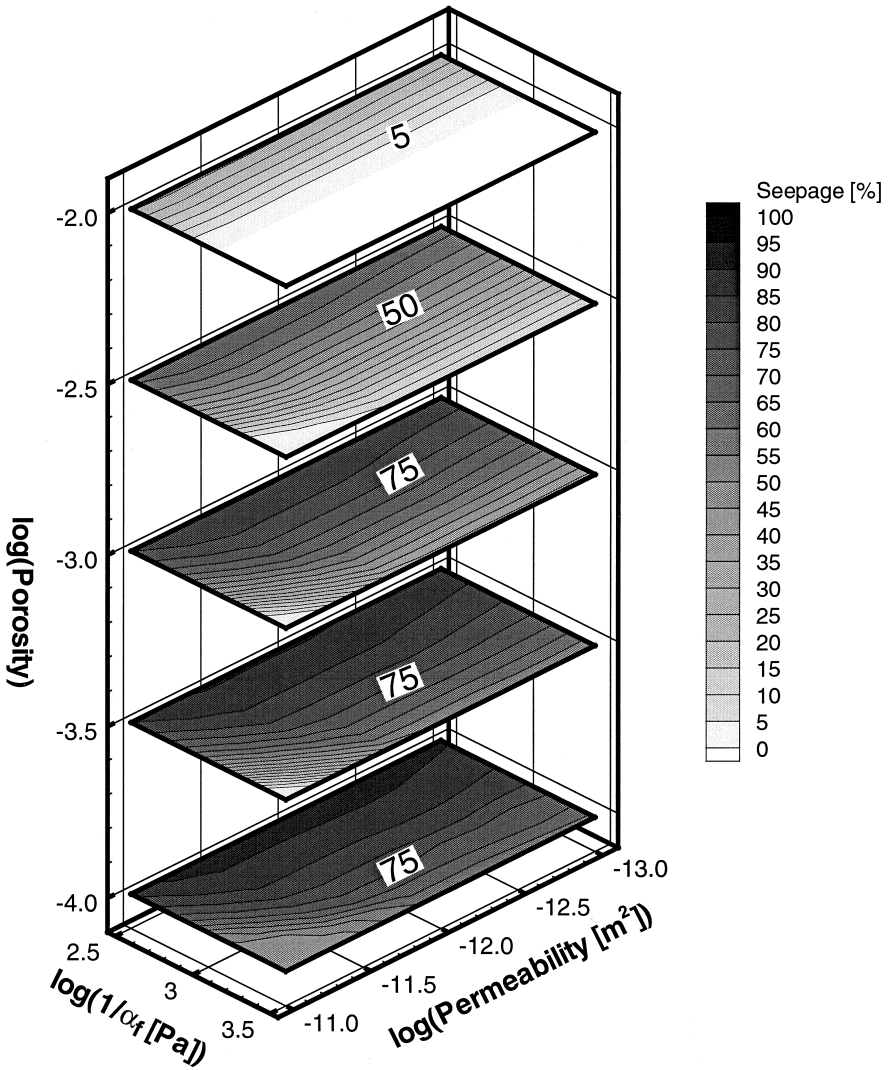

Fig. 11. Total seepage (after 1 day) as a function of fracture permeability, capillarity, and porosity.

capacity of the fractures, reduces the seepage, as illustrated in the set of contour graphs along the vertical axis. Strong capillarity, as measured by the van Genuchten parameter $1/\alpha_f$, promotes water retention by the fractures and reduces seepage.

For a given porosity and capillarity, the seepage is only sensitive to permeability in the high permeability range, as illustrated in Fig. 12, for both two-dimensional and three-dimensional models. High permeability values do not induce high seepage. The injected liquid can be effectively diverted around the niche with a high fracture permeability in the rock. The diversion reduces the likelihood of local ponding at the

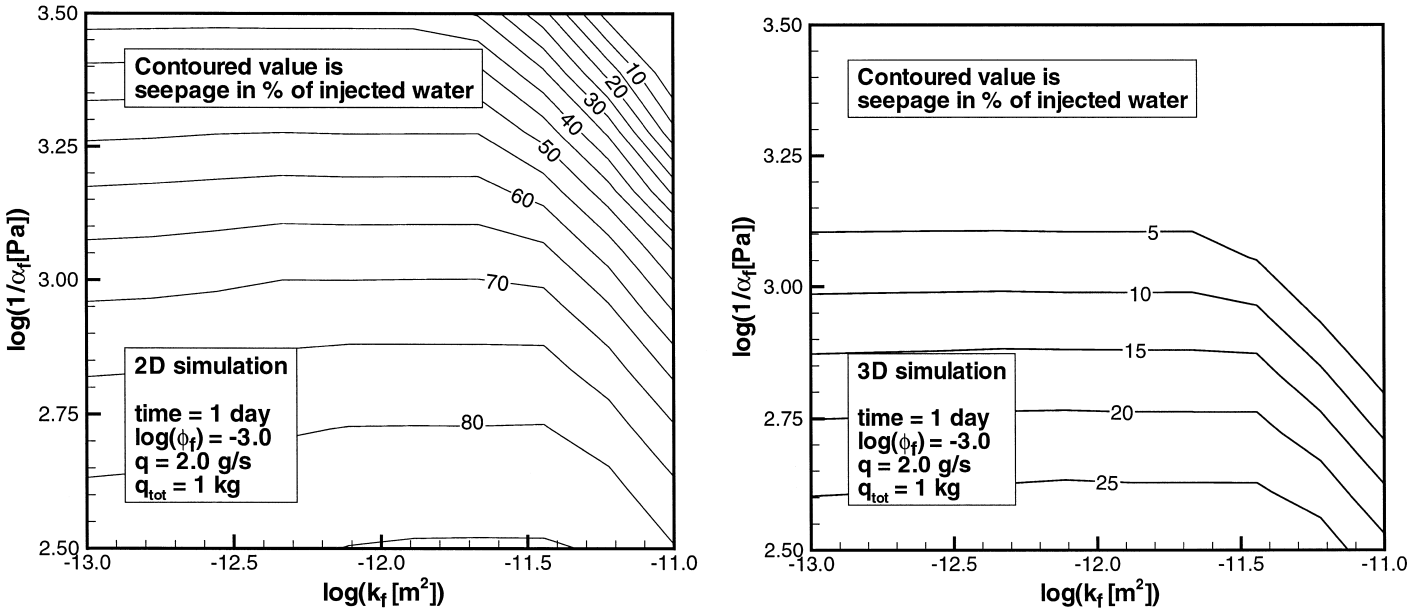

Fig. 12. Seepage percentage as a function of fracture permeability k and capillarity parameter $1/\alpha_f$ assuming two-dimensional (left) and three-dimensional (right) fracture continuum.

niche boundary. Fig. 12 also illustrates that the seepage in three-dimensional models, representing fracture network with multiple fracture paths, is lower than seepage in two-dimensional models, representing flow limited to discrete fracture planes.

8. Discussion and summary

This paper focuses on field test results and model analyses of the first set of five niche seepage tests conducted at Niche 3650. The results suggested that (1) the niche opening acts as a capillary barrier; (2) a seepage threshold exists; and (3) the seepage is a fraction of the liquid released above the niche ceiling.

The flow path characterizations were conducted in three stages: before, during, and after niche excavation. Air injection tests were used to measure the spatial distribution of fracture permeability. Nearly two-order-of-magnitude changes in air permeability values were measured before and after niche excavation in 0.3-m (1-ft) long borehole test intervals. Alternation of fracture flow paths due to excavation and proximity of the niche open boundary could contribute to the permeability changes. Liquid release tests were conducted at selected borehole intervals with nominally 1000 g or less of dyed water injected at minimal pressure (0–5 cm head) for pre-excavation characterization of the fracture flow paths, and for post-excavation quantification of seepage into niche. The dyed flow paths, together with a wet feature potentially associated with an ambient flow path, were mapped during dry excavation operations. The ambient flow paths could be fairly localized as observed at Niche 3566.

The excavation-induced changes in fracture flow paths also increase the rates and amounts of liquid mass in some borehole intervals. For cases with seepage dripping observed, the wetting fronts of the post-excavation liquid release tests with fluorescent dyes were observed to shift from the food dye stained areas of pre-excavation flow paths on the niche ceiling. Migration of water along the ceiling surface, imbibition into other small fractures, and local accumulation of water were observed before dripping, including a case near seepage threshold with wetting front observed to reach the niche ceiling but no dripping occurred.

The seepage is quantified by the ratio of the water mass dripped into a niche to the mass released above the opening at selected borehole intervals. The first set of tests of post-excavation liquid release tests to quantify seepage was conducted at the Niche 3650 site, with ratios range from 0% (no dripping for two tests) to 27.2%. Test results were analyzed with drift scale models, using measured air permeability values as input parameters and two-dimensional and three-dimensional conceptualizations to represent discrete fracture and fracture network for the flow paths. Simple model results, with parameters consistent with the unsaturated zone site scale model, are able to interpret the test results without additional parameter fitting. For the three tests with measurable seepage, two tests can be interpreted with three-dimensional fracture-network-continuum models, and the third test result (in a borehole interval with high permeability) can be interpreted with an effectively two-dimensional model to represent discrete fractures.

Sensitivity analyses were performed to improve the understanding of the seepage processes. The seepage is sensitive to the niche boundary conditions, with capillary

barrier conditions generating close matches and free draining conditions (without requirement of local saturated conditions) overestimating the seepage percentages. For the distances and durations of the niche seepage tests, the seepage is moderately sensitive to the heterogeneity of the fracture flow paths and to the strengths of matrix imbibition. All flow paths observed are associated with fractures, with minimal matrix imbibition detected from grab rock samples. Test results and sensitivity analyses indicate that strong capillary strength and large storage capacity of the fracture flow paths limit the seepage. High permeability value also reduces seepage if the liquid release rate is smaller than the hydraulic conductivity of the flow path.

The models used to simulate the tests are very simple. Homogeneous representations of the fractures and fracture network essentially reproduce the test results, in terms of total seepage percentage, transient times of arrival, and dripping duration. These preliminary results of field tests and model analyses of the first set of five niche seepage tests at one niche could be used to guide better design of tests in the ESF to improve understanding of the seepage distribution, capillary barrier mechanism, and other flow and transport processes which are important for the performance assessment of waste isolation in the unsaturated zone at Yucca Mountain.

Acknowledgements

We thank Yvonne Tsang and Chin-Fu Tsang for their technical reviews and comments for improvement. We thank Alan Mitchell and his colleagues of the ESF Test Coordination Office for the field support at ESF, and for the coordination with the ESF Constructor for drilling and excavation operations. This work was supported by the Director, Office of Civilian Radioactive Waste Management, US Department of Energy, through Memorandum Phase Order EA9013MC5X between TRW Environmental Safety Systems and Ernest Orlando Lawrence Berkeley National Laboratory (Berkeley Lab.). The support is provided to Berkeley Lab. through the US Department of Energy Contract No. DE-AC03-76SF00098.

References

Birkholzer, J., Tsang, C.F., 1997. Solute channeling in unsaturated heterogeneous porous medium. Water Resour. Res. 33 (10), 2221–2238.

Birkholzer, J., Li, G., Tsang, C.F., Tsang, Y., 1999. Modeling studies and analysis of seepage into drifts at Yucca Mountain. J. Contam. Hydrol. 38.

Bodvarsson, G.S., Bandurraga, T.M., Haukwa, C., Sonnenthal, E.L., Wu, Y.S., 1997. The site scale unsaturated zone model of Yucca Mountain, for the viability assessment. Yucca Mountain Project Milestone Report LBNL-40376. Lawrence Berkeley National Laboratory, Berkeley, CA.

Bodvarsson, G.S., Boyle, W., Patterson, R., Williams, D., 1999. Overview of scientific investigations at Yucca Mountain—the potential repository for high-level nuclear waste. J. Contam. Hydrol. 38.

Fabryka-Martin, J.T., Turin, H.J., Wolfsberg, A.V., Brenner, D., Dixon, P.R., Musgrave, J.A., 1996. Summary report of chlorine-36 studies. Milestone 3782M, LA-CST-TIP-97-003. Los Alamos National Laboratory, Los Alamos, NM.

Finsterle, S., 1997. ITOUGH2 command reference, LBL-40041. Lawrence Berkeley National Laboratory, Berkeley, CA.

LeCain, G.D., 1995. Pneumatic testing in 45-degree-inclined boreholes in ash-flow tuff near Superior, Arizona. U.S. Geological Survey Water Resources Investigations Report 95-4073, Denver, CO.

Montazer, P., Wilson, W.E., 1984. Conceptual hydrologic model of flow in the unsaturated zone, Yucca Mountain, Nevada. U.S. Geological Survey Water-Resources Investigations Report 84-4345, Lakewood, CO.

Nitao, J.J., Buscheck, T.A., Chesnut, D.A., 1992. The implications of episodic nonequilibrium fracture-matrix flow on site suitability and total system performance. Proceedings of the Third Annual International High Level Radioactive Waste Management Conference, Vol. 1, pp. 279–296.

Oldenburg, C.M., Pruess, K., 1993. On numerical modeling of capillary barriers. Water Resour. Res. 29 (4), 1045–1056.

Philip, J.R., 1989a. The seepage exclusion problem for sloping cylindrical cavities. Water Resour. Res. 25 (6), 1447–1448.

Philip, J.R., 1989b. Asymptotic solutions for the seepage exclusion problem for elliptic-cylindrical, spheroidal, and strip- and disc-shaped cavities. Water Resour. Res. 25 (7), 1531–1540.

Philip, J.R., 1990. Some general results on the seepage exclusion problem. Water Resour. Res. 26 (3), 369–377.

Philip, J.R., Knight, J.H., Waechter, R.T., 1989a. Unsaturated seepage and subterranean holes: conspectus, and exclusion problem for cylindrical cavities. Water Resour. Res. 25 (1), 16–28.

Philip, J.R., Knight, J.H., Waechter, R.T., 1989b. The seepage problems for parabolic and paraboloidal cavities. Water Resour. Res. 25 (4), 605–618.

Pruess, K., Narasimhan, T.N., 1985. A practical method for modeling fluid and heat flow in fractured porous media. Soc. Petrol. Eng. J. 25 (1), 14–26.

Ross, B., 1990. The diversion capacity of capillary barriers. Water Resour. Res. 26 (10), 2625–2629.

Tsang, Y.W., Tsang, C.F., Hale, F.V., 1996. Tracer transport in a stochastic continuum model of fractured media. Water Resour. Res. 32 (10), 3077–3092.

Tsang, C.F., Li, G., Birkholzer, J., Tsang, Y.W., 1997. Drift Scale Abstraction: Additional Results on Seepage into Drifts and Model Testing against Liquid Release Test, Milestone NWD98-2. Lawrence Berkeley National Laboratory, Berkeley, CA.

van Genuchten, M.T., 1980. A close-form equation for predicting the hydraulic conductivity of unsaturated soil. Soil Sci. Soc. Am. J. 44 (5), 892–898.

Wang, J.S.Y., Narasimhan, T.N., 1985. Hydrologic mechanisms governing partially saturated fluid flow in fractured porous medium. Water Resour. Res. 21 (12), 1861–1874.

Wang, J.S.Y., Cook, N.G.W., Wollenberg, H.A., Carnahan, C.L., Javandel, I., Tsang, C.F., 1993. Geohydrologic data and models of Rainier Mesa and their implications to Yucca Mountain. Proceedings of the Fourth Annual International High Level Radioactive Waste Management Conference, Vol. 1, pp. 675–681.

Wang, J.S.Y., Cook, P.J., Trautz, R.C., Salve, R., James, A.L., Finsterle, S., Tokunaga, T.K., Solbau, R., Clyde, J., Flint, A., Flint, L., 1997. Field testing and observation of flow paths in niches, phase 1 status report of the drift seepage test and niche moisture study. Yucca Mountain Project Milestone SPC314M4, Lawrence Berkeley National Laboratory, Berkeley, CA.

Webb, S.W., 1997. Generalization of Ross tilted capillary barrier diversion formula for different two-phase characteristic curves. Water Resour. Res. 33 (8), 1855–1859.